Scaling of fracture length and distributed damage

Vladimir Lyakhovsky

The Institute of Earth Sciences, The Hebrew University of Jerusalem, Givat Ram, Jerusalem 91904, *Israel. E-mail: vladi@cc.huji.ac.il*

SUMMARY

The linear theory of elasticity formulated in terms of dimensionless strain components does not allow the introduction of any space scaling except linear relations between fracture length and displacements and thus the determination theoretically of the strength of a body or structure directly. Self-similarity of a fracture process means the existence of a universal faulting mechanism. However, the general applicability of universal scaling to field observations and rock mechanics measurements remains the subject of some debate. Complete self-similarity of a fracture process is hardly ever found experimentally, except in some aluminium alloys. At early stages of the loading, material degrades due to increasing microcrack concentrations. Later, these microcracks where distributed in the process zone localize into a subcritically growing macrocrack, and finally the fracture process accelerates and rupture runs away, producing dynamic fracture. The macroscopic effects of distributed cracking and other types of damage require treatment by constitutive models that include non-linear stress–strain relations together with material degradation and recovery. The present model treats two physical aspects of the brittle rock behaviour: (1) a mechanical aspect, that is, the sensitivity of the macroscopic elastic moduli to distributed cracks and to the type of loading, and (2) a kinetic aspect, that is, damage evolution (degradation/recovery of elasticity) in response to ongoing deformation. To analyse the scaling of a fracture process and the onset of the dynamic events, we present here the results of numerical modelling of mode I crack growth. It is shown that the distributed damage and the process zone created eliminate the stress–strain crack-tip singularities, providing a finite rate of quasi-static crack growth. The growth rate of these cracks fits well the experimentally observed power law, with the subcritical crack index depending on the ratio between the driving force and the confining pressure. The geometry of the process zone around a quasi-static crack has a self-similar shape identical to that predicted by universal scaling of the linear fracture mechanics. At a certain stage, controlled by dynamic weakening and approximated by the reduction of the critical damage level proportional to the rate of a damage increase, the self-similarity breaks down and crack velocity significantly deviates from that predicted by the quasi-static regime. The subcritical crack growth index increases steeply, crack growth accelerates, the size of the process zone decreases, and the rate of crack growth ceases to be controlled by the rate of damage increase. Furthermore, the crack speed approaches that predicted by the elastodynamic equation. The model presented describes transition from quasi-static crack propagation to the dynamic regime and gives proper time and length scales for the onset of the catastrophic dynamic process.

Key words: fracture zone, rheology, rupture propagation.

INTRODUCTION

Some of the fractures or fracture zones in the Earth's crust were probably created in quasi-static regimes as a result of the slow propagation and joining of microcracks, while others formed during earthquakes or in dynamic regimes. Under some conditions, a quasi-static crack may accelerate, or a fracture front may run away, producing a dynamic fracture. Although this may be common in nature, classical fracture mechanics does not provide a means for determining theoretically the transition between quasi-static and dynamic regimes. The reason is that the theory of elasticity is linear and is formulated in

114

terms of small strain components. Moreover, these strain components are dimensionless and it is therefore not possible to introduce scaling, except for linear relations between fracture lengths and displacements (Scholz *et al.* 1993). Such scaling is compatible with field observations that suggest the size of the process zone grows proportionally to the fracture length (Vermilye & Scholz 1998). Although this observation is in violation of the premises of the critical stress intensity factor approach (Rubin 1995a,b), it is decisively documented around dykes that form by the injection of magma into fractures (Delaney *et al.* 1986; Baer 1991; Weinberger *et al.* 1995; Hoek 1995). However, the general applicability of the universal scaling remains the subject of some debate. The length of the process zone around the tip of a propagating fracture, as well as the fracture energy and toughness, are functions of the specimen or of the structure size and shape (e.g. Bazant & Kazemi 1990). Sinclair & Chambers (1987) have reviewed the experimental evidence of the size effect. Field observations of two populations of tensile fractures in the Krafla fissure swarm of northeast Iceland clearly show the breaking of self-similarity and the non-universal scaling of fracture length and aperture (Hatton *et al.* 1994; Renshaw & Park 1997).

Laboratory investigations of fracturing show that this process cannot be described in terms of the propagation of a single crack (e.g. Yukutake 1989; Lockner *et al.* 1991; Reches & Lockner 1994). The finite size effect of the fracture process zone is often treated with models that specify a cohesive zone near the crack tip within the plane of the crack (Dugdale 1960; Barenblatt 1962; Ida 1972; Palmer & Rice 1973; Rubin 1993; Willemse & Pollard 1998). However, in most engineering and rock-like materials, a slowly propagating crack is preceded by an evolving out-of-plane process zone around its tip (e.g. Bazant & Cedolin 1991; Lockner *et al.* 1991). The distributed damage modifies the elastic coefficients in the medium around the tip and hence controls the macrocrack trajectory and the growth rate (Huang *et al.* 1991; Chai 1993; Zietlow & Labuz 1998). Thus, it is desirable to account specifically for the out-of-plane inelastic deformation around the propagating crack.

A rheological model of an elastic material with distributed damage reproduces the main features of subcritical crack growth under constant and cyclic loading (fatigue). The object of this paper is to show that such a model simulates the fracture process that controls the transition between quasi-static and dynamic regimes, and introduces temporal and spatial scaling. It also reproduces the breaking of scaling.

SUBCRITICAL CRACK GROWTH

Classical fracture mechanics postulates that an isolated crack will propagate at velocities approaching the speed of sound in the medium once a critical stress intensity factor, K_{CR}, has been reached or exceeded at the crack tip (Irwin 1958). At lower stress intensity factors, the crack remains stable. A more general approach in classical fracture mechanics is to consider the strain energy release rate, G, during crack extension (e.g. Freund 1990). Dynamic crack extension occurs when G reaches a critical value G_{CR}.

These classical models have been used successfully to predict catastrophic crack propagation in metals, ceramics and glasses. In grainy materials, however, the stress field is highly non-uniform at the grain scale. When such materials are subjected

to long-term loading, they show considerable rates of macroscopic crack extension at values of K and G significantly lower than the critical values. This phenomenon is known as subcritical crack growth (Swanson 1984; Atkinson & Meredith 1987; Ingraffea 1987; Cox & Scholz 1988).

The rates of subcritical crack growth are most commonly represented by a power law equation (Charles 1958),

$$\frac{dL}{dt} = A_1 K_I^m, \tag{1a}$$

or by the Paris & Erdogan (1963) law for a cycling load,

$$\frac{dL}{dn} = A_2 (\Delta K_I)^m, \tag{1b}$$

where L is the crack length, t is time, n is the number of cycles and K_I is the mode I stress intensity factor or its amplitude in the loading cycle. The values A_1, A_2 and the subcritical crack growth index, m, are material parameters that depend on the confining pressure, temperature and chemical environment (that is, the presence of an active pore fluid and its chemical activity). Eqs (1a) and (1b) are well established by engineering and rock mechanics experiments and reflect a self-similarity in the fracture process that relates the rate of crack growth to its length,

$$\frac{dL}{dt} = A_3 L^{m/2}. \tag{1c}$$

For a constant remote stress, K_I is approximated by $\sqrt{L}$, and A_3 is set equal to A_1 or A_2 multiplied by the remote stress to the power of m. For $m=2$, the growth law $d\ln(L)=A_3 dt$ is completely scale-independent. This 'complete similarity', in terms of Barenblatt (1996), is hardly ever found, except in some aluminium alloys.

Experimental observations of fracture propagation (e.g. Meredith & Atkinson 1985; Collins 1993) and indirect calculation of the *m*-values from microseismic data (Main *et al.* 1992; 1993) indicate that plots of fracture propagation rate versus its length can generally be divided into three segments (Fig. 1). Propagation probably starts with $m=2$ in the very slow crack corrosion regime (region I) and increases up to about 5. In rocks, the exponent m decreases in region II, where crack behaviour is controlled by the rate of transport of reactive species to the crack tip. This regime typically does not exist in the fracturing of metals. The rupture in regime III is largely independent of chemical environment and therefore m increases steeply in this region.

In the following sections, it is shown that the rate of quasi-static crack propagation in a material governed by damage rheology fits eq. (1) for m varying from 2 to 5 with increasing confining pressure. The relation between the rate of fracture process and material strength, introduced in the model as dynamic weakening, is responsible for the transition to regime III and further crack acceleration up to the dynamic regime. The model does not include any type of reactive species transport and thus cannot describe regime II of rock behaviour.

DAMAGE RHEOLOGY

In this section, the main features of the damage rheology model are presented. Detailed explanations and comparisons with rock mechanic experiments may be found in Lyakhovsky *et al.* (1997a,b).
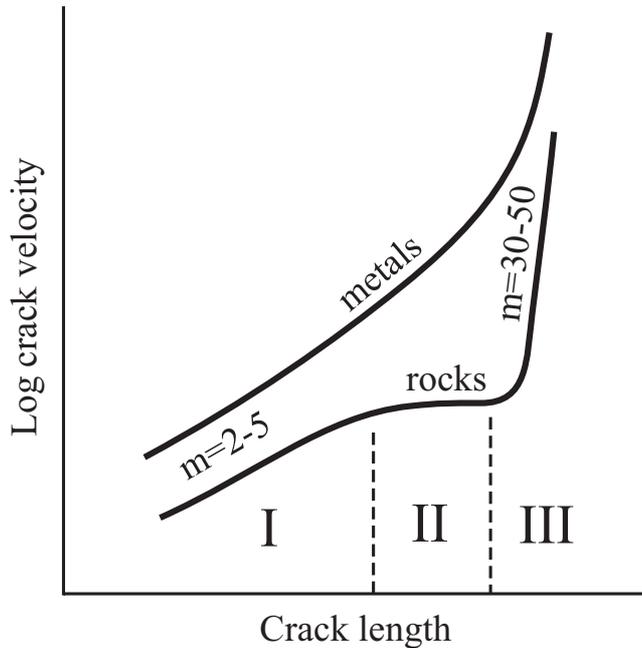
Figure 1. Typical relation between crack length and crack growth rate. The curve is divided into three sections, each representing a different mechanism limiting the fracture growth rate.

The cumulative effect of distributed microcracks and flaws in the elastic material leads to non-linearity, which is described by an energy potential equation of the form:

$$U = \frac{1}{\rho}\left(\frac{\lambda}{2} I_1^2 + \mu I_2 - \gamma I_1 \sqrt{I_2}\right), \tag{2}$$

where ρ is the density, $I_1 = \varepsilon_{ii}$, $I_2 = \varepsilon_{ij}\varepsilon_{ij}$ are two invariants of the strain tensor ε_{ij}, and λ, μ and γ are Lame parameters. The energy expression eq. (2) includes a new non-analytical, second-order term in addition to the quadratic terms containing invariants of the strain tensor of the Hookean elastic solid. The effect of variable damage is introduced by making the Lame parameters a function of the damage level α (that is, $\lambda(\alpha)$, $\mu(\alpha)$ and coupling coefficient $\gamma(\alpha)$, $0 \leq \alpha \leq 1$). The variable α can be envisioned as the density of microcracks in a laboratory specimen or as the density of small faults in a crustal domain. In damage-free material ($\alpha = 0$), the coupling coefficient γ vanishes and the energy potential is Hookean. The coefficient γ increases with material degradation and achieves its maximum for totally destroyed material ($\alpha = 1$). According to the equation in Murnaghan (1951), the stress tensor, σ_{ij}, is defined as the derivative of the energy potential with respect to the strain tensor,

$$\sigma_{ij} = \rho\frac{\partial U}{\partial \varepsilon_{ij}} = \left(\lambda - \frac{\gamma}{\xi}\right)I_1\delta_{ij} + 2\left(\mu - \frac{1}{2}\gamma\xi\right)\varepsilon_{ij}. \tag{3}$$

The non-zero coupling coefficient γ makes the effective elastic moduli dependent on the strain diagonality, $\xi = I_1/\sqrt{I_2}$, which varies from $-\sqrt{3}$ for 3-D compaction to $\sqrt{3}$ for 3-D tension. $\xi = \pm 1$ means uniaxial tension or compression, respectively, and $\xi = 0$ — zero volumetric strain ($I_1 = 0$).

The amount of damage evolves in time as a result of an applied load. Using the balance equations of the energy and entropy, and accounting for irreversible changes related to viscous deformation and material damage, the equation of

damage evolution has the form (Lyakhovsky *et al.* 1997a)

$$\frac{d\alpha}{dt} = -C\frac{\partial U}{\partial \alpha}, \tag{4}$$

where C is a positive function of the state variables describing the temporal rate of the damage process. It must be emphasized that this approach describes not only damage increase but also a process of material recovery associated with healing of microcracks, which is favoured by high confining pressure, low shear stress and high temperature. Agnon & Lyakhovsky (1995) chose the moduli μ and γ to be linear functions of α (i.e. $\mu = \mu_0 - \alpha\mu_r$, $\gamma = \alpha\gamma_r$) and the modulus λ be constant. The values of μ_r, γ_r are calculated from the condition of material destruction for $\alpha = 1$ (eq. 15 from Lyakhovsky *et al.* 1997a). The latest analysis of laboratory acoustic emission and stress–strain data, and their comparison to theoretical modelling, confirms this assumption (Liu *et al.* 1999). Increasing the added modulus γ from zero for linear elastic damage-free material to its maximum value at critical damage amplifies the material non-linearity with damage accumulation. Lyakhovsky *et al.* (1997a) suggested that the damage rate equation has different forms for weakening and for healing. These are, respectively,

$$\frac{d\alpha}{dt} = \begin{cases} C_d I_2(\xi - \xi_0), & \text{for} \quad \xi \geq \xi_0 \\ C_1 \exp[\alpha/C_2]I_2(\xi - \xi_0), & \text{for} \quad \xi \leq \xi_0 \end{cases}. \tag{5}$$

Both equations include an adjustable parameter ξ_0 that indicates the transition stage from strengthening to degradation. Agnon & Lyakhovsky (1995) and Lyakhovsky *et al.* (1997a) related this parameter to the angle of internal friction by considering the critical shear stress for Mohr–Coulomb sliding. They found $\xi_0 = -0.8$ for typical ratios of elastic moduli for damage-free material $\lambda/\mu \sim 1$ (Poisson's ratio of 0.25) and an internal friction angle $\sim 40°$ (eq. 37 and Fig. 3 of Lyakhovsky *et al.* 1997a). This value varies little for different rocks with Poisson's ratios between 0.2 and 0.3 and is used for the following numerical simulations. The parameter C_d is the damage rate constant, which defines the time needed to achieve failure after the onset of damage at $\xi = \xi_0$. C_d is assumed to be a material property and its value has been estimated to vary from 0.5 to 5 s^{-1} for different rocks tested at more than 20 MPa confining pressure and room temperature (Lyakhovsky *et al.* 1997a). This parameter certainly depends on temperature and chemical environment, two factors that are not simulated in this paper. It might also be pressure-dependent, especially at low confining pressures. Making the damage rate for healing proportional to the exponent of the current damage level (α) gives logarithmic-in-time material recovery that mimics the logarithmic-in-time increase of the static friction with the duration of stationary contact, as reported by Dieterich (1972) and others. This allows us to relate the constants C_1 and C_2, which describe the rate of healing, to the coefficients of the experimental static friction law (Lyakhovsky *et al.* 1997a).

When deformation in some region achieves a threshold state ($\xi = \xi_0$), the damage starts to increase, weakening the material element. The weakening ends when the damage level becomes critical and stress drop occurs [see eqs 14 and 15 and Fig. 1 of Lyakhovsky *et al.* (1997a) for the relation between the critical damage α_{cr} and strain diagonality ξ]. The brittle failure leads to an increase of non-reversible plastic deformation, corresponding to the non-reversible slip in models that approximate the fault structure as a plane. During failure, the local deviatoric

stresses of the destroyed element drop to zero, keeping only the confining component. This is supported by laboratory experiments (e.g. Brune *et al.* 1993), theoretical models (e.g. Heaton 1990; Mora & Place 1994; Andrews & Ben-Zion 1997) and a variety of geophysical observations (see Ben-Zion & Andrews 1998 for a summary). After failure, the stress conditions in the post-failure region favour healing, which may last until the next failure event. The duration of the cycle between previous and subsequent failure depends on the rate of loading and material recovery.

The real dynamic process, wherein waves are generated by the stress drop, is not simulated here. However, a quasi-dynamic procedure is applied to simulate a rupture front propagation. This is accomplished by recalculating the stress field after each stress drop in every element involved in the rupture process, and by incorporating dynamic weakening of material; the latter is achieved by reducing the critical value of the damage parameter, α_{cr}, to $\alpha_{dynamic}$:

$$\alpha_{dynamic} = \alpha_{cr} - \sqrt{\tau_a \frac{d\alpha}{dt}}, \qquad (6)$$

where τ_a is a material parameter. The condition $\alpha = \alpha_{cr}$ means that the material does not support any static load. Mathematically this criterion corresponds to a loss of convexity of the elastic energy U (eq. 2) or to a zero elastic modulus in the 1-D case. In reality, this condition can be achieved only if damage increase is infinitesimally slow. Damage increase at a finite rate causes the amplification of elastic waves. Using the linear relation between elastic moduli and damage level, the characteristic time of this amplification is $(\alpha_{cr} - \alpha)^2/(d\alpha/dt)$. However, waves are attenuated with characteristic time τ_a, which is related to a Q parameter of the medium ($\tau_a \sim Q/f$, where f is frequency) (Aki & Richards 1980). While the amplification makes the system dynamically unstable, the attenuation brings the system back to the stable regime. The dynamic instability occurs when these processes have the same effect, or when α is slightly below the α_{cr} corrected after the rate of damage increase and attenuation. A detailed derivation of eq. (6) and its consequences are given in Agnon *et al.* (1997, 1999).

GROWTH OF MODE I CRACK UNDER CONFINING PRESSURE

Consider a mode I crack embedded in an infinite elastic solid governed by damage rheology. Assume that the crack lies in a horizontal plane and propagates in its own direction (Fig. 2). The crack starts to grow from a small notch (0.03 of the area length) in a damage-free material. Stress concentration around the crack tip results in a build-up of a process zone or a zone where the damage is non-zero ($\alpha > 0$). When the damage in front of the crack tip achieves its critical value, the crack length increases and previously destroyed elements form a crack boundary. Thus, a post-failure zone (a zone where plastic strain is accumulated and the material effectively behaves as a gouge zone governed by healing) surrounds the crack.

The entire system—crack and surrounding material—is subjected to a certain confining pressure, P_c, and tensional driving force, F_d, acting in the direction perpendicular to the crack plane and applied at infinity. The upper boundary of the simulated area is placed far from the process zone, where the damage-free material behaves as linear elastic. However, it
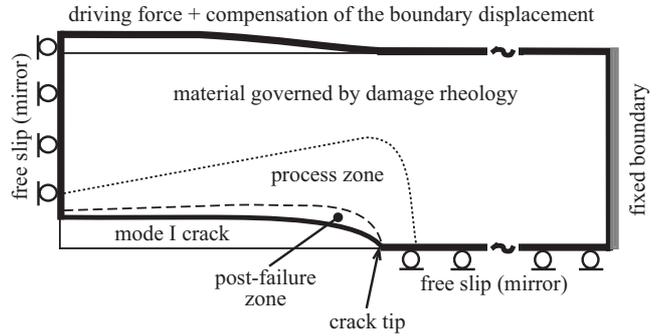
Figure 2. The problem set-up for numerical simulation of crack propagation. The variable force vector, F_i (eq. 7), applied to each node at the top boundary, corresponds to the constant traction force, F_d, applied infinitely far from the simulated region. Each element is subjected to the initial confining pressure P_c.

is not placed far enough to ignore the effect of the boundary condition and the directly applied constant traction F_d. Such an increase of the simulated area is computationally too expensive. Instead, this boundary is allowed to be displaced and the applied boundary forces, F_i, compensate the linear elastic deformation of the outer space between the numerical boundary and infinity. The time and space variable force vector corresponding to the constant uniform traction applied infinitely far from the simulated area is calculated according to the linear elasticity equation

$$F_i = F_d + \frac{\mu_0}{\pi(1-v)} \int_{-\infty}^{\infty} \frac{\partial u_i}{\partial x} \frac{d\varsigma}{x-\varsigma}, \qquad (7)$$

where F_d is a driving force per unit area applied at infinity, F_i and u_i are the boundary force and displacement, respectively, μ_0 is the shear modulus and v is the Poisson's ratio of the damage-free material. The formulation of the problem suggests mirror symmetry with respect to the crack plane and a vertical line splitting the crack into two halves. These two lines with free-slip conditions bound the simulated area (Fig. 2). The right edge of the simulated area is placed far enough from the crack tip (maximum crack length is 0.3 of the area size) and therefore the zero displacement boundary condition has negligibly small effect on stress distribution inside. The FLAC algorithm, modified for damage rheology, is used for the simulations (Weinberger *et al.* 1999).

The velocity of quasi-static, damage-controlled crack propagation depends on the rate of damage increase. The timescale of the damage increase, t_d, is defined by the kinetics of the damage process (Meriaux *et al.* 1999),

$$t_d = \left(\frac{\mu_0}{F_d}\right)^2 \frac{1}{c_d}. \qquad (8)$$

Numerical simulations for different ratios between the driving force and confining pressure (P_c/F_d) are scaled with t_d. The results are presented below. If the driving force, F_d, is three orders of magnitude below the rigidity, μ_0, of the damage-free material ($\varepsilon \sim 10^{-3}$ far from the crack tip) and $c_d = 1 \text{ s}^{-1}$, then the timescale, t_d, is 10^6 s. Therefore, the initial 10^{-3} m notch should propagate with a velocity of the order of 10^{-9} m s^{-1}. This value is close to the lower boundary of the observed subcritical crack velocity, which ranges from 10^{-2} to $10^{-10} \text{ m s}^{-1}$ (Swanson 1984; Swanson 1987; Atkinson & Meredith 1987; Cox & Scholz 1988).

The kinetics of the damage process allows the introduction of a timescale for the fracture process; nevertheless, as in linear elasticity, it does not provide a clear length scale. Thus, results of simulations are scaled with the length of the initial notch. Scale-dependent behaviour and definition of the critical length derive from the dynamic weakening equation (6) and are discussed in the following section.

RESULTS OF SIMULATIONS

Stress and strain crack-tip singularity

As is well known from linear elasticity, loading of the crack walls as well as remote loading in damage-free elastic material produce crack-tip stress and strain singularities. Stress (Fig. 3a) and strain (Fig. 3b) distributions (circles) around the initial notch prior to the damage onset perfectly fit an analytical solution (heavy line) that decreases as $r^{-1/2}$ with distance r
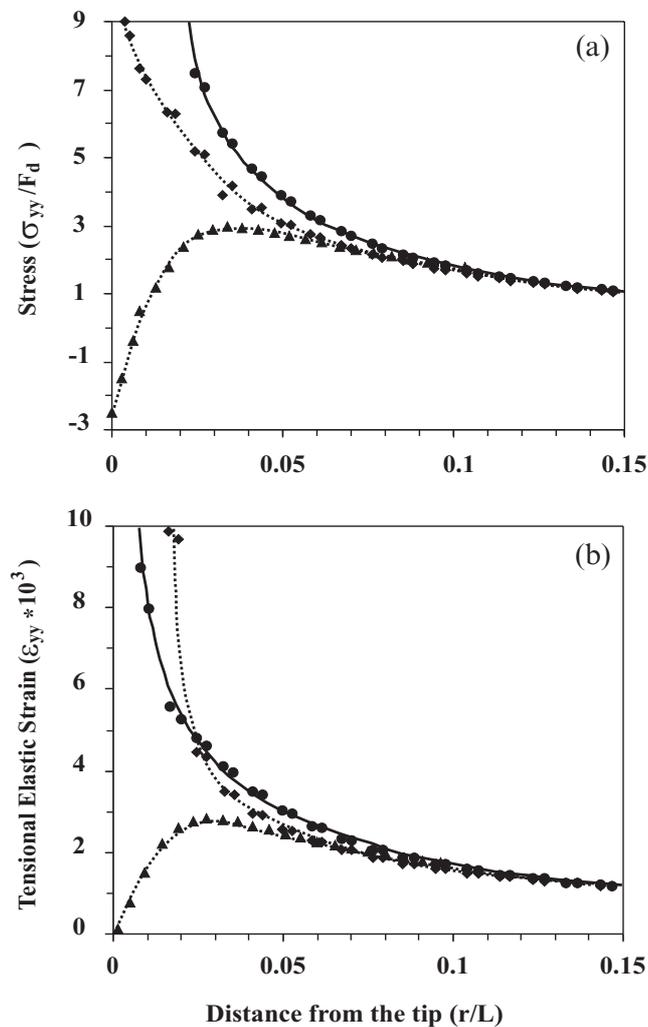
Figure 3. The process zone around the crack eliminates tip singularity for stress (a) and strain (b) distribution (triangles). Circles represent the stress (a) and strain (b) distributions prior to the onset of damage; this configuration fits perfectly an analytical solution (heavy line). Diamonds correspond to the stress (a) and strain (b) distributions around a crack surrounded by a process zone without the post-failure zone (prior to the onset of crack propagation).

from the crack tip. In agreement with the analytical results of Meriaux *et al.* (1999), increasing the damage and build-up of the process zone prior to failure regularizes the stress distribution and amplifies the strains (diamonds in Fig. 3). Stresses in the process zone ($r < 0.1L$) fall below the $r^{-1/2}$ line, while the strains steeply increase at small distances. The strain value is already twice as large as the classical analytical solution for $r = 0.017L$. Further damage increase up to a critical value and consequent stress drop lead to the formation of a post-failure zone that accumulates plastic strains. This zone around the propagating crack not only eliminates the stress singularity, but also regularizes the elastic part of the total deformation. Stress at the crack tip (triangles in Fig. 3a) drops to the confining pressure (-2.5 for the simulation presented), where the tensional elastic strain vanishes (triangles in Fig. 3b). The stress and strain increase and achieve a maximum at a distance of about $0.03L$. They approach the linear elastic solution and coincide with it outside the process zone at a distance of $r > 0.1L$. This stress–strain distribution is similar to that predicted by the Barenblatt–Dugdale model of a crack with a cohesive zone near the tip (Dugdale 1960; Barenblatt 1962; Rubin 1993; Willemse & Pollard 1998).
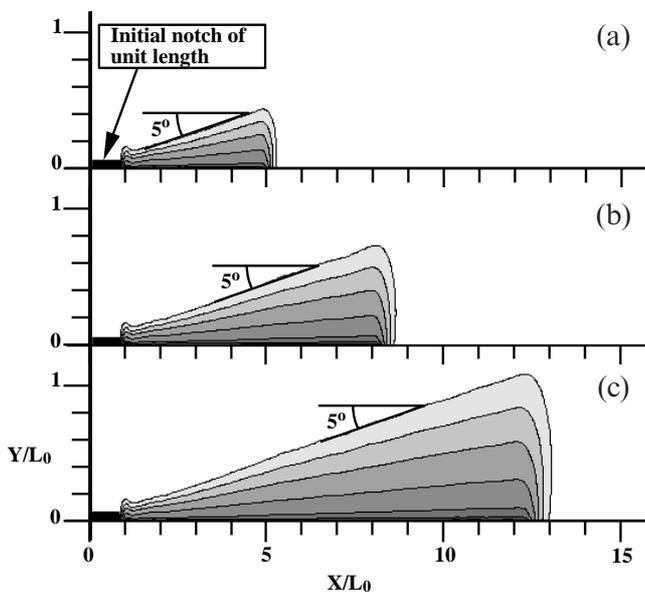
Quasi-static crack growth

The regularization of the stress and strain tip singularity allows the growth rate for the quasi-static damage-controlled crack propagation to be correctly defined. Results of numerical simulations (Fig. 4) with different ratios between confining pressure and driving force (P_c/F_d) fit the power law equation (1c) well for crack length changes of one order of magnitude (from 0.03 to 0.3 of the area size). The velocity of the longer cracks is below that predicted by the power law equation (not shown here); this is probably the effect of the proximity of the fixed boundary on the right. The subcritical crack growth index increases from $m = 2.6$–3.5 as the ratio P_c/F_d increases from 1.5 to 3.5 (Fig. 4). The material properties used in this and other simulations are $\xi_0 = -0.8$, $C_d = 1$ s^{-1}, $C_1 = 10^{-8}$, $C_2 = 0.05$, $\mu_0 = \lambda$ (Poisson's ratio of 0.25) and $\mu_0/F_d = 10^{-3}$. According to eq. (8), the timescale, t_d, is equal to 10^6 s.

Based on the results of compression acoustic emission tests with intact rocks, Main *et al.* (1993) presented four experimental values for the subcritical crack growth index (Figs 10I–iv in their paper): $m = 3.5, 2.7, 2.8, 2.4$. The theoretically obtained range ($m = 2.6$–3.5) perfectly fits the experimental values; however, it is not clear whether the experimental results confirm or contradict the theoretically predicted increase in subcritical crack growth index with increasing confining pressure. It is also problematic to compare the theoretically derived values with experimental results from different authors who used different rocks (Westerly granite and Darley-Dale sandstone) under different experimental conditions.

These simulations are carried out under the inviscid limit, where the relaxation time is much shorter than the damage timescale ($t_d \gg \tau_a$). Hence, self-similarity for quasi-static crack growth is preserved. In spite of the incomplete similarity ($m > 2$), the size of the process zone increases proportionally to the crack length, except for a small perturbation at the initial stage that forms a bulge at the tip of the initial notch. All the isodamage lines behind the crack tip are nearly straight and have the same slope (compare Figs 5a, b and c). The slope of the outer boundary of the process zone is about 5° for different
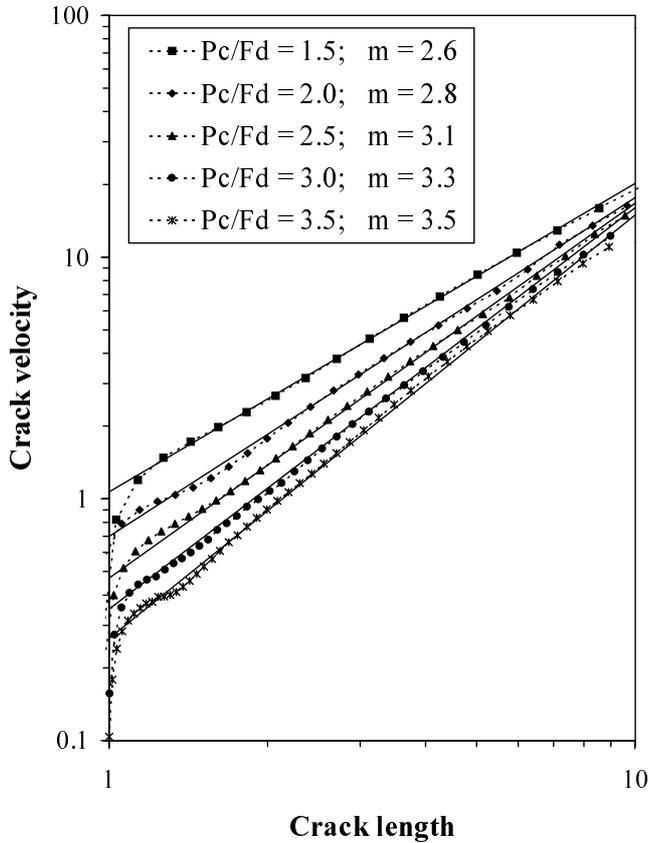
Figure 4. Log–log plot of the crack velocity versus the length of the quasi-static propagating crack for different ratios of confining pressure to driving force (P_c/F_d). The numerical solutions (dotted lines with markers) fit the power law equation (1c) (straight lines with slope $m/2$) well, representing increasing subcritical crack growth index (m) as a result of increasing confining pressure.

stages of the crack growth. This slope and the related size of the process zone around the crack decrease with increasing confining pressure (Fig. 6). The maximum size of the process zone, characterized by a 15° slope of the outer boundary, was obtained for the lowest confining pressure, $P_c/F_d = 1.5$ (Fig. 6a); the minimum size, characterized by a 2.5° slope, corresponds to $P_c/F_d = 3.5$ (Fig. 6c). This tendency corresponds to the expected increase of the area with high tensile stress around the crack tip with decrease of the confining pressure. The strain diagonality for an extensional driving force and zero confining pressure, uniaxial tension, is equal to $\xi = +1$, which is above the critical value $\xi_0 = -0.8$. Thus, uniaxial tension produces a simultaneous damage increase everywhere, because the condition for damage onset ($\xi > \xi_0$) is satisfied in the whole plate, not only in the vicinity of the pre-existing notch. In this case the vertical size of the simulated area should be significantly increased, which makes proper numerical analysis of the unconfined crack growth impossible. In this case, the self-similarity is probably complete with the subcritical crack growth index $m = 2$.
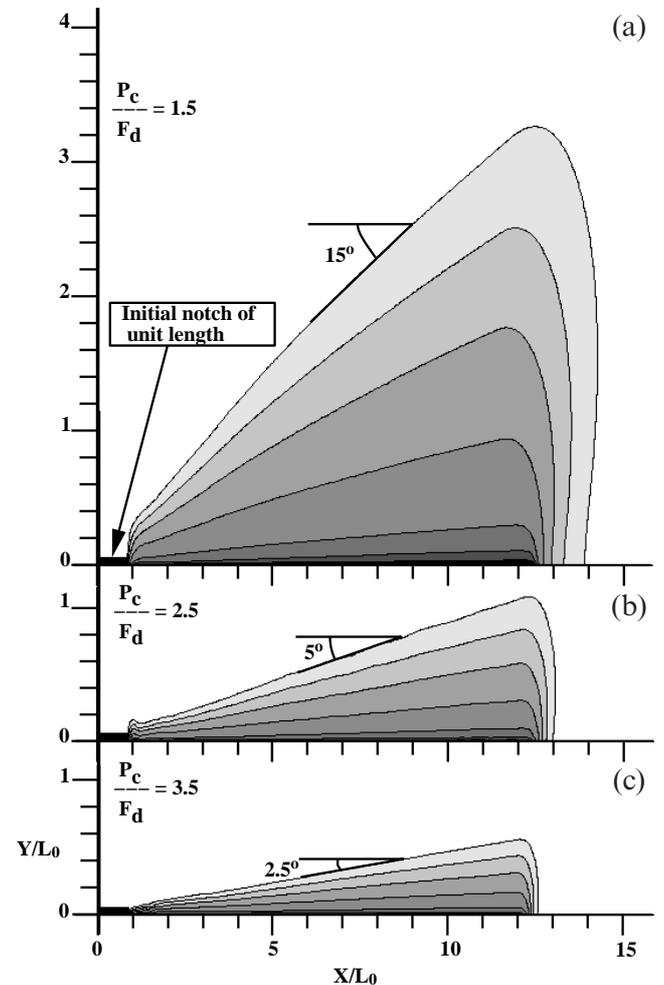
Figure 6. The size of the process zone around a crack of the same length as in Fig. 5 depends on the ratio between confining pressure and driving force (P_c/F_d). (a) Lower confining pressure ($P_c/F_d = 1.5$) corresponds to the largest process zone, which has a 15° slope of the outer boundary; (b) medium-sized process zone with 5° slope corresponds to $P_c/F_d = 2.5$, as in Fig. 5(c); (c) minimum-sized process zone with 2.5° slope corresponds to $P_c/F_d = 3.5$.

Figure 5. The process zone for three different stages of quasi-static crack growth ($P_c/F_d = 2.5$) has a self-similar geometry with a constant 5° slope of the outer boundary. Here and in Figs 6 and 8 the step between contour levels is 0.1.
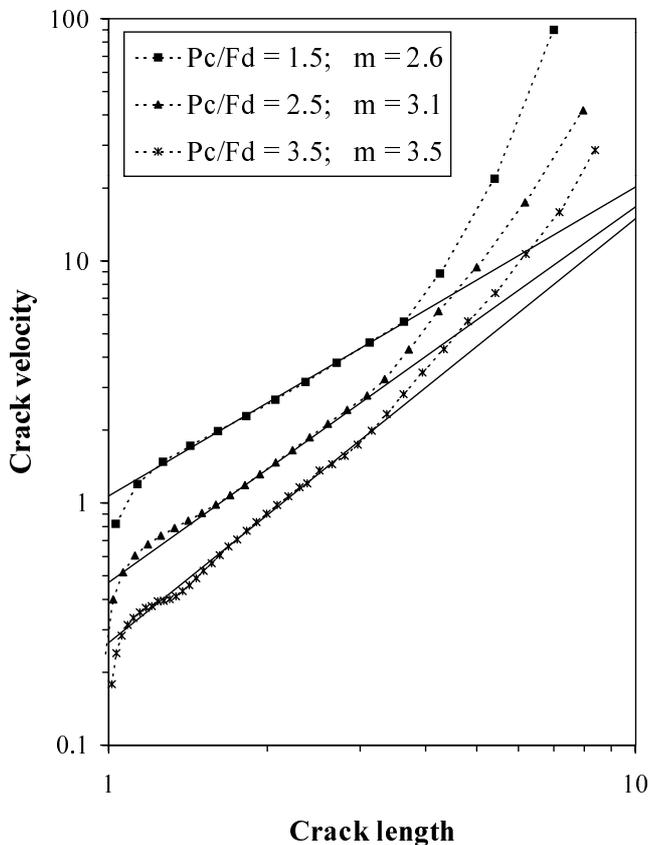
Effect of dynamic weakening

The proportional increase of the process zone with crack length indicates that the damage rate around the propagating crack fits the power law with the same index m as the crack growth equation (1c),

$$\frac{d\alpha}{dt} = \frac{B}{t_d} L^{m/2}, \tag{9}$$

and a dimensional coefficient B depending on the confining pressure. Eq. (9), together with the equation for the dynamic weakening (6), allows the definition of the upper boundary of the crack length, L_{cr}, for a crack propagating in the quasi-static self-similar regime described by eqs (1a) and (1b),

$$L_{cr} = \left(\frac{B\tau_a}{t_d}\right)^{(-2/m)}. \tag{10}$$

Substituting eq. (10) into eq. (9) and then into eq. (6) gives zero critical damage ($\alpha_{cr} = 0$) for the crack length equal to L_{cr}. Consequently, a process zone is not created around the crack tip, the quasi-static regime is impossible and the crack propagates in the dynamic regime governed by an elasto-dynamic equation (e.g. Freund 1990). This transition is shown in Fig. 7 for simulated crack growth with $\tau_a = 30 t_d$. All other material and geometrical parameters are the same as in the quasi-static case. Crack velocity (dotted lines with markers) follows the power law of the quasi-static regime (heavy lines taken from Fig. 4) until the crack length becomes 2–4 times its initial length. Dynamic weakening starts to decrease the critical damage value and crack growth accelerates in a similar manner to stage III of Fig. 1. This acceleration cannot be related to the proximity of the boundary on the right because it has an opposite effect, slowing down much longer cracks. When crack velocity approaches the speed of elastic waves, the crack growth ceases to be controlled by the damage process.

The process zone around the crack changes its shape due to the dynamic weakening (Fig. 8). Prior to the significant reduction in critical damage (Fig. 8a), it is similar to that around a quasi-static crack (Fig. 5a). Further reduction of the critical damage decreases the size of the process zone (Fig. 8b). The slope of the outer boundary of the process zone behind the crack tip is much lower and some of the internal isodamage lines have negative slope. This tendency is amplified with further crack acceleration (Fig. 8c), reducing the process zone size to zero. Thus, the process zone of the dynamically propagating crack is very small, or does not exist at all.

DISCUSSION

The damage rheology model outlined above is based on thermodynamic principles and fundamental observations of rock deformation. Its advantage over other crack propagation models is that it provides the time and spatial scaling of the fracture process and reproduces the main features of subcritical crack growth under constant and cycling loads, including transition between a quasi-static and a dynamic regime. The results of the theoretical and numerical analyses of mode I crack growth can be summarized as follows.
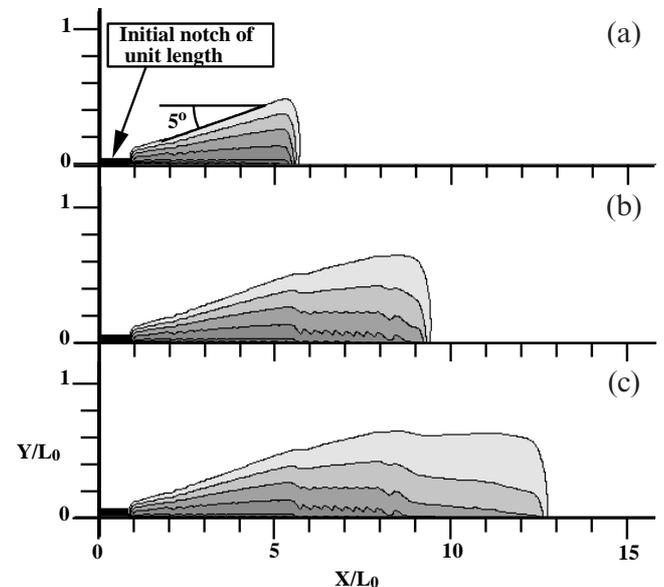

Figure 7. Dynamic weakening with $\tau_d = 30 t_d$ (dotted lines with markers) breaks the self-similarity quasi-static propagation (straight lines from Fig. 4) when the crack length reaches 2–4 times its initial length. At this stage the dynamic weakening significantly decreases the critical value of the damage density; crack growth accelerates and ceases to be controlled by the damage process.

Figure 8. The process zone around the crack corresponding to the ratio ($P_c/F_d = 2.5$) has the same geometry until the dynamic weakening is negligible (a). The size of the process zone increases much more slowly when the dynamic weakening becomes important (b), and even decreases at the crack acceleration stage (c).

Crack-tip singularity. Positive damage evolution starts when the strain becomes critical, leading to gradual damage in a process zone. The results of the near-tip analysis show that the stress singularity is regularized by a damage model relative to the linear elasticity (Meriaux *et al.* 1999). However, the strain singularity is amplified at the initial stage of the damage evolution, which lasts until a critical damage value is reached and stress drop occurs. Stress drop and accumulation of plastic deformation in the post-failure zone not only regularize stress, but also eliminate strain singularity. The equations of stress have a regular solution at every point, including at the crack tip. These solutions provide the finite rate of quasi-static crack growth.

Quasi-static crack growth. The theoretically derived rate of quasi-static crack growth fits the experimentally observed power law (eq. 1) well, with the subcritical crack growth index depending on the ratio between the driving force and confining pressure. The numerical results presented here correspond to subcritical crack growth indexes ranging from 2.6 to 3.5, depending on the confining pressure. This variation falls within the experimentally observed range (2–5) and is comparable with the range characteristic of subcritical crack growth in the crack corrosion regime (stage I in Fig. 1).

Process zone. The geometry of the process zone around a quasi-static crack has a self-similar shape identical to the universal scaling of linear fracture mechanics. The size of the process zone depends not only on the driving force and material properties, but also on the confining pressure. Increasing the confining pressure results in decreasing the process zone. This explains why the same rocks under the same differential loading produce narrow fault zones under high confining pressure, and wide zones of distributed damage under low confining or unconfined conditions.

Critical crack length. The dynamic weakening decreases the critical damage value and leads to acceleration of the crack growth. When dynamic weakening reduces the critical damage to zero, the process zone vanishes and the crack propagates in a dynamic regime. This allows the introduction of the critical length (eq. 10), which depends on the relaxation time, τ_a; in turn, the relaxation time is related to the attenuation of the elastic waves, which is proportional to the Q parameter. Under the loading corresponding to the same quasi-static growth rate (same t_d and B as in eq. 10), the critical length decreases with Q as $L_{cr} \sim Q^{-2/m}$. Therefore, the critical length is expected to be significantly smaller for granite than for sandstone, as demonstrated in the laboratory study of quasi-static fault growth (Lockner *et al.* 1992) due to high attenuation in the latter material. Thus, the model predicts the existence of a narrow zone in granite that formed by relatively few fast-propagating cracks in a transitional or dynamic regime, and numerous distributed quasi-static cracks in sandstone, where every nucleus remains stable for a longer time.

The fracture process in rocks decelerates at the transition between stages I and III (stage II). Stage II is usually considered to be controlled by the rate of transport of reactive species to the crack tip; therefore, this stage does not exist in the fracture process of metals, in which the role of fluids is minor. In rock fracturing, however, fluids probably play a significant role. Although this factor is not considered in the model discussed above, future improvements of the model may introduce damage–fluid interaction in order to understand the effect of fluids on the rate of rupture front propagation.

CONCLUSIONS

The damage rheology model of brittle rocks predicts the existence of two different regimes of fracture growth: quasi-static damage-controlled growth and dynamic growth. The rate of quasi-static crack propagation fits the power law with small subcritical crack growth index ($m = 2$–5) well. At a certain stage, controlled by dynamic weakening and approximated by the condition given by eq. (10), the self-similarity breaks down and crack velocity significantly deviates from that predicted by the quasi-static regime. The subcritical crack growth index increases steeply, crack growth accelerates, the size of the process zone decreases, and the rate of crack growth ceases to be controlled by the rate of damage increase. Furthermore, the crack speed approaches that predicted by the elastodynamic equation. The model presented above, which includes a reduction of the critical level of damage due to dynamic weakening, describes the transition from fracture regime I to regime III and sets proper time and length scales for the fracture process.

REFERENCES

Agnon, A. & Lyakhovsky, V., 1995. Damage Distribution and Localization During Dyke Intrusion, in *The Physics and Chemistry of Dykes,* pp. 65–78, eds Baer, G. & Heimann, A., Balkema, Rotterdam.

Agnon, A., Lyakhovsky, V. & Ben-Zion, Y., 1997. Localization of distributed damage and strain to stick-slip faults, in *Localization Phenomena and Dynamics of Brittle and Granular Systems*, pp. 33–39, ed. Scholz, C.H., Columbia University, NY.

Agnon, A., Lyakhovsky, V. & Ben-Zion, Y., 2000. A continuum approach to rock friction, *Earth planet. Sci. Lett.,* in press.

Aki, K. & Richards, P.G., 1980. *Quantitative Seismology, Theory and Methods,* W. H. Freeman, San Francisco, CA.

Andrews, D.J. & Ben-Zion, Y., 1997. Wrinkle-like slip pulse on a fault between different materials, *J. geophys. Res.,* **102,** 553–571.

Atkinson, B.K. & Meredith, P.G., 1987. The theory of subcritical crack growth with applications to minerals and rocks, in *Fracture Mechanics of Rock,* pp. 110–166, ed. Atkinson, B.K., Academic Press, San Diego.

Baer, G., 1991. Mechanisms of dike propagation in layered rocks and in massive, porous sedimentary rocks, *J. geophys. Res.,* **96,** 11 911–11 929.

Barenblatt, G.I., 1962. Mathematical theory of equilibrium cracks in brittle fracture, in *Advances in Applied Mechanics,* 55–129, Academic, San Diego, CA.

Barenblatt, G.I., 1996. *Scaling, Self-Similarity. and Intermediate Asymptotics,* Cambridge University Press, Cambridge.

Bazant, Z.P. & Cedolin, L., 1991. *Stability of Structures, Elastic, Inelastic, Fracture and Damage Theories,* Oxford University Press, Oxford.

Bazant, Z.P. & Kazemi, M.T., 1990. Determination of fracture energy, process zone length and brittleness number from size effect, with application to rock and concrete, *Int. J. Fract.,* **44,** 111–131.

Ben-Zion, Y. & Andrews, D.J., 1998. Properties and implications of dynamic rupture along a material interface, *Bull. seism. Soc. Am.,* **88,** 1085–1094.

Brune, J.N., Brown, S. & Johnson, P.A., 1993. Rupture mechanism and interface separation in foam rubber model of earthquakes: a possible solution to the heat flow paradox and the paradox of large overthrusts, *Tectonophysics,* **218,** 59–67.

Chai, H., 1993. Observation of deformation and damage at the tip of cracks in adhesive bonds loaded in shear and assessment of a criterion for fracture, *Int. J. Fract.,* **60,** 311–326.

Charles, R.J., 1958. Static fatigue of glass, *J. appl. Physics,* **29,** 1549–1560.

Collins, J.A., 1993. *Failure of Materials in Mechanical Design,* John Wiley, New York.

Cox, S.J.D. & Scholz, C.H., 1988. Rupture initiation in shear fracture of rocks: an experimental study, *J. geophys. Res.,* **93,** 3307–3320.

Delaney, P.T., Polard, D.D., Ziony, J.I. & McKee, E.H., 1986. Field relations between dikes and joints: emplacement processes and paleostress analysis, *J. geophys. Res.,* **91,** 4920–4938.

Dieterich, J.H., 1972. Time-dependent friction in rocks, *J. geophys. Res.,* **77,** 3690–3697.

Dugdale, D.S., 1960. Yielding of steel sheets containing slits, *J. Mech. Phys. Solids,* **8,** 100–104.

Freund, L.B., 1990. *Dynamic Fracture Mechanics,* Cambridge University Press, Cambridge.

Hatton, C.G., Main, I.G. & Meredith, P.G., 1994. Non-universal scaling of fracture length and opening displacement. *Nature,* **367,** 160–162.

Heaton, T.H., 1990. Evidence for and implications of the self-healing pulses of slip in earthquake rupture, *Phys. Earth planet. Inter.,* **64,** 1–20.

Hoek, J.D., 1995. Dyke propagation and arrest in proterozoic tholeitic dyke swarms, Vestfold Hills, East Antarctica, in *The Physics and Chemistry of Dykes,* pp. 79–95, eds Baer, G. & Heimann, A., Balkema, Rotterdam.

Huang, W.-L., Kunin, B. & Chudnovsky, A., 1991. Kinematics of damage zone accompanying curved crack, *Int. J. Fract.,* **50,** 143–152.

Ida, Y., 1972. Cohesive force across the tip of longitudinal shear crack and Griffith's specific surface energy, *J. geophys. Res.,* **77,** 3796–3805.

Ingraffea, A.R., 1987. Theory of crack initiation and propagation in rock, in *Fracture Mechanics of Rock,* pp. 76–110, ed. Atkinson, B.K., Academic Press, San Diego.

Irwin, G.R., 1958. Elasticity and plasticity, in *Handbuch der Physic,* Vol. VI, pp. 551–590, ed. Flugge, S., Springer, Berlin.

Liu, Y., Lyakhovsky, V., Ben-Zion, Y. & Lockner, D., 1999. Analysis of acoustic emission and stress-strain laboratory data with a damage rheology model, *Fall AGU Mtng.*

Lockner, D.A., Byerlee, J.D., Kuksenko, V., Ponomarev, A. & Sidorin, A., 1991. Quasi-static fault growth and shear fracture energy in granite, *Nature,* **350,** 39–42.

Lockner, D.A., Byerlee, J.D., Kuksenko, V., Ponomarev, A. & Sidorin, A., 1992. Observations of quasi-static fault growth from acoustic emission, in *Fault Mechanics and Transport Properties of Rocks, International Geophysics Series,* Vol. 51, pp. 3–31, eds Evans, B. & Wong, T.-F., Academic Press, San Diego.

Lyakhovsky, V., Ben-Zion, Y. & Agnon, A., 1997a. Distributed damage, faulting, and friction, *J. geophys. Res.,* **102,** 27 635–27 649.

Lyakhovsky, V., Reches, Z., Weinberger, R. & Scott, T.E., 1997b. Non-linear elastic behavior of damaged rocks, *Geophys. J. Int.,* **130,** 157–166.

Main, I.G., Meredith, P.G. & Sammonds, P.R., 1992. Temporal variations in seismic event rate and b-values from stress corrosion constitutive laws, *Tectonophysics,* **211,** 233–246.

Main, I.G., Meredith, P.G. & Sammonds, P.R., 1993. Application of a modified Griffith criterion to the evolution of fractal damage during compressional rock failure, *Geophys. J. Int.,* **115,** 367–380.

Meredith, P.G. & Atkinson, B.K., 1985. Fracture toughness and subcritical crack growth during high-temperature tensile deformation of Westerly granite and Black gabbro, *Tectonophysics,* **39,** 33–51.

Meriaux, C., Lister, J.R., Lyakhovsky, V. & Agnon, A., 1999. Dyke propagation with distributed damage of the host rock, *Earth planet. Sci. Lett.,* **165,** 177–185.

Mora, P. & Place, D., 1994. Simulation of the frictional stick-slip instability, *Pure appl, Geophys.,* **143,** 61–87.

Murnaghan, F.D., 1951. *Finite Deformation of an Elastic Solid,* John Wiley, New York.

Palmer, A.C. & Rice, J.R., 1973. The growth of slip surfaces in the progressive failure of over-consolidated clay, *Proc. R. Soc. Lond.,* **A332,** 527–548.

Paris, P.C. & Erdogan, F., 1963. A critical analysis of crack propagation laws, *J. Basic Engineering, ASME Trans.,* Series D, **85,** 528–534.

Reches, Z. & Lockner, D.A., 1994. Nucleation and growth of faults in brittle rocks, *J. geophys. Res.,* **99,** 18 159–18 173.

Renshaw, C.E. & Park, J.C., 1997. Effect of mechanical interactions on the scaling of fracture length and aperture, *Nature,* **386,** 482–484.

Rubin, A.M., 1993. Tensile fracture of rock at high confining pressure: implications for dike propagation, *J. geophys. Res.,* **98,** 15 919–15 935.

Rubin, A.M., 1995a. Propagation of magma filled cracks, *Ann. Rev. Earth planet. Sci.,* **8,** 287–336.

Rubin, A.M., 1995b. Why geologists should avoid using "fracture toughness" (at least for dikes), in *The Physics and Chemistry of Dykes,* pp. 53–65, eds Baer, G. & Heimann, A., Balkema, Rotterdam.

Scholz, C.H., Dawers, N.H., Yu, J.-Z., Anders, M.H. & Cowie, P.A., 1993. Fault growth and fault scaling laws: preliminary results, *J. geophys. Res.,* **98,** 21 951–21 961.

Sinclair, G.B. & Chambers, A.E., 1987. Strength size effect and fracture mechanics: what does the physical evidence say?, *Eng. Fract. Mech.,* **26,** 279–310.

Swanson, P.L., 1984. Sub critical crack growth and other time and environment-dependent behavior in crustal rocks, *J. geophys. Res.,* **89,** 4137–4152.

Swanson, P.L., 1987. Tensile fracture resistance mechanisms in brittle polycrystals: an ultrasonics and in situ microscopy investigation, *J. geophys. Res.,* **92,** 8015–8036.

Vermilye, J.M. & Scholz, C.H., 1998. The process zone: a micro-structural view of fault growth, *J. geophys. Res.,* **103,** 12 223–12 236.

Weinberger, R., Baer, G., Shamir, G. & Agnon, A., 1995. Deformation bands associated with dyke propagation in porous sandstone, Makhtesh Ramon, Israel, in *The Physics and Chemistry of Dykes,* pp. 95–115, eds Baer, G. & Heimann, A., Balkema, Rotterdam.

Weinberger, R., Lyakhovsky, V. & Agnon, A., 1999. Damage evolution and propagation path of en-echelon cracks, in *Rock Mechanics for Industry,* pp. 1125–1143, eds Amadei, B., Kranz, R.L., Scott, G.A. & Smealie, P.H., Balkema, Rotterdam.

Willemse, E.J.M. & Pollard, D.D., 1998. On the orientation and patterns of wing cracks and solution surfaces at the tips of a sliding flaw or fault, *J. geophys. Res.,* **103,** 2427–2438.

Yukutake, H., 1989. Fracturing process of granite inferred from measurements of spatial and temporal variations in velocity during triaxial deformation, *J. geophys. Res.,* **94,** 15 639–15 651.

Zietlow, W.K. & Labuz, J.F., 1998. Measurements of the intrinsic process zone in rock using acoustic emission, *Int. J. Rock Mech. Min. Sci.,* **35,** 291–299.